Chiral Monolayers with Achiral Tetrapod Molecules on Highly Oriented Pyrolytic Graphite

著者	Asakawa Hitoshi, Matsui Sayaka, Trinh Quang Than, Hirao Hajime, Inokuma Yasuhide, Ogoshi Tomoki, Tanaka Saki, Komatsu Kayo, Ohta Akio, Asakawa Tsuyoshi, Fukuma Takeshi
著者別表示	淺川 雅, 生越 友樹, 太田 明雄, 淺川 毅, 福間 剛士
journal or publication title	Journal of Physical Chemistry C
volume	124
number	14
page range	7760-7767
year	2020-04-09
URL	http://doi.org/10.24517/00065563

doi: 10.1021/acs.jpcc.9b11246

THE JOURNAL OF PHYSICAL CHEMISTRY C

pubs.acs.org/JPCC Article

Chiral Monolayers with Achiral Tetrapod Molecules on Highly Oriented Pyrolytic Graphite

Hitoshi Asakawa,* Sayaka Matsui, Quang Thang Trinh, Hajime Hirao, Yasuhide Inokuma, Tomoki Ogoshi, Saki Tanaka, Kayo Komatsu, Akio Ohta, Tsuyoshi Asakawa, and Takeshi Fukuma

Cite This: J. Phys. Chem. C 2020, 124, 7760–7767 Read Online

ACCESS | Metrics & More | Article Recommendations | Supporting Information

ABSTRACT: The self-assembly of organic molecules at the surface of highly oriented pyrolytic graphite (HOPG) is a promising process for constructing molecular-scale architectures. However, selectable organic molecules are generally restricted to two-dimensional molecules with planar π-conjugated structures and alkyl chains. We herein present the formation of self-assembled monolayers of tetrakis(4-ethynylphenyl)methane (TEPM) having a three-dimensional (3D) tetrapod geometry on HOPG, which was achieved by utilizing a simple spin-coating method. The arrangements of TEPM molecules in the monolayers were investigated using frequency-modulation atomic force microscopy (FM-AFM). The resulting subnanometer-resolution FM-AFM images revealed that the TEPM molecules formed linear rows with a periodicity of 0.85 nm oriented in a parallel configuration but with two alternating intervals of 0.7 and 1.0 nm. Moreover, the TEPM monolayers were classified into two chiral types with a relationship of mutual mirror-image symmetry, according to the observed molecular arrangements. Our results demonstrate the capability of TEPM molecules to act as 3D building blocks for the design of molecular-scale architectures at interfaces.

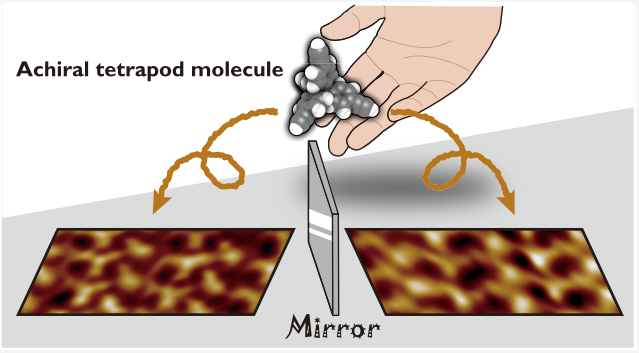

INTRODUCTION

The self-assembly of organic molecules at interfaces has attracted considerable attention as a bottom-up approach to constructing molecular-scale architectures. Although such self-assembled structures have been obtained using a range of organic molecules,[1,2] systematic design of the interfacial architectures remains a challenge. In addition, atomically flat substrates have been used as platforms for constructing two-dimensional (2D) self-assembled monolayers with key examples including highly oriented pyrolytic graphite (HOPG), which is a suitable platform for the assembly of organic molecules consisting of planar π-conjugated structures, alkyl chains, and their combinations.[2−9] Indeed, the design of chiral surfaces based on molecular self-assembly has been identified as a major goal due to their demand for use in applications such as chiral specific separation and sensing.[10−17] Previous studies have demonstrated that not only chiral organic molecules but also achiral molecules can form chiral structures on HOPG.[11,14,15,17] Thus, to develop sophisticated chiral surfaces based on molecular self-assembly, a systematic methodology for precise molecular design should be established. However, the number of selectable organic molecules that have been reported to form self-assembled monolayers is limited with the majority consisting of 2D frameworks with planar π-conjugated structures and alkyl chains. The energetically favorable orientations of such 2D organic molecules tend to be parallel to the basal plane of HOPG. Thus, a novel family of organic molecules that can extend the chemical structure vertically from the surface toward three-dimensional (3D) interfacial spaces is required to establish a systematic methodology for the molecular design. In this context, we wished to explore an organic molecule that exhibits a 3D extended structure and is able to form a self-assembled monolayer on HOPG. Here, we present our study into the formation of self-assembled monolayers of tetrakis(4-ethynylphenyl)methane (TEPM) molecules on HOPG. Unlike 2D organic molecules, a TEPM molecule consisting of four equivalent ethynylphenyl groups presents a 3D tetrapod geometry with high structural rigidity (Figure 1). When three equivalent ethynylphenyl groups act as anchoring sites for binding to the HOPG surface, the remaining ethynylphenyl group has a perpendicular arrangement with respect to the surface. Although its high lateral resolution has brought

Received: December 3, 2019
Revised: March 13, 2020
Published: March 18, 2020

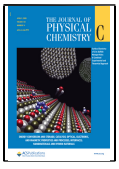

https://dx.doi.org/10.1021/acs.jpcc.9b11246
J. Phys. Chem. C 2020, 124, 7760–7767

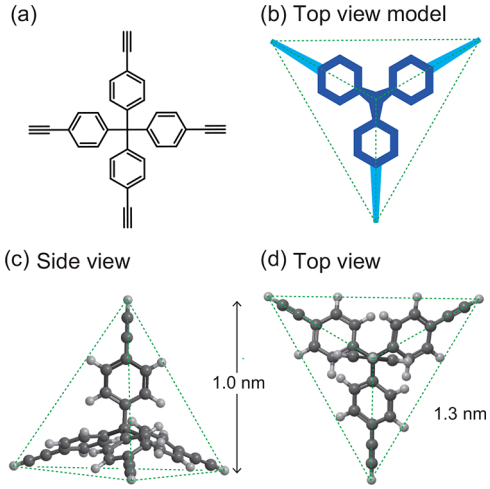

Figure 1. (a) Chemical structure of TEPM. (b) Top view of a simplified illustration of a TEPM molecule. (c) Side view and (d) top view of the 3D tetrahedral (tetrapod) structure of a TEPM molecule. The height (from the basal plane to an apical hydrogen atom) and the side length of the tetrahedral structure are approximately 1.0 and 1.3 nm, respectively.

scanning tunneling microscopy (STM) into wide use to investigate molecular-scale arrangements of self-assembled monolayers formed from various organic molecules on HOPG, STM investigations of spatially extended organic molecules exhibiting non-conducting properties are challenging. Indeed, the STM tips may cause deformation and destruction of TEPM molecules and self-assembled structures because of their large molecular sizes (*i.e.*, >1 nm). In this study, we employed frequency-modulation atomic force microscopy (FM-AFM), which is a technique that allows us to visualize subnanometer-scale structures even in the presence of fragile structures such as proteins.[18−20] The obtained FM-AFM images suggested the formation of self-assembled monolayers of TEPM molecules on HOPG. Further, the adsorption energies of the TEPM molecules on the HOPG surface in different configurations were calculated using a density functional theory (DFT) approach. These experimental and theoretical studies provided molecular-scale insights into the arrangement and orientation of the TEPM molecules on HOPG and revealed the formation of two chiral structures with a relationship of mutual mirror-image symmetry.

METHODS

Preparation of Self-Assembled Monolayers of TEPM on HOPG. TEPM powder (1.0 mg, T3151, Tokyo Chemical Industry Co., Ltd.) was dissolved in chloroform (2.4 mL) (infinity pure, 033-15721, FUJIFILM Wako Pure Chemical Corporation) to prepare a stock solution (1 mM). This stock solution was subjected to ultrasonication for 1 min and subsequently diluted with chloroform to a concentration of 0.6 mM prior to each experiment. The HOPG substrate (SPI-1 grade, 7 mm × 7 mm, SPI Supplies) was cleaved using a tape and then rotated on a spin coater (MS-B100, MIKASA Co., Ltd.) at 7000 rpm. A drop of the prepared TEPM solution (6

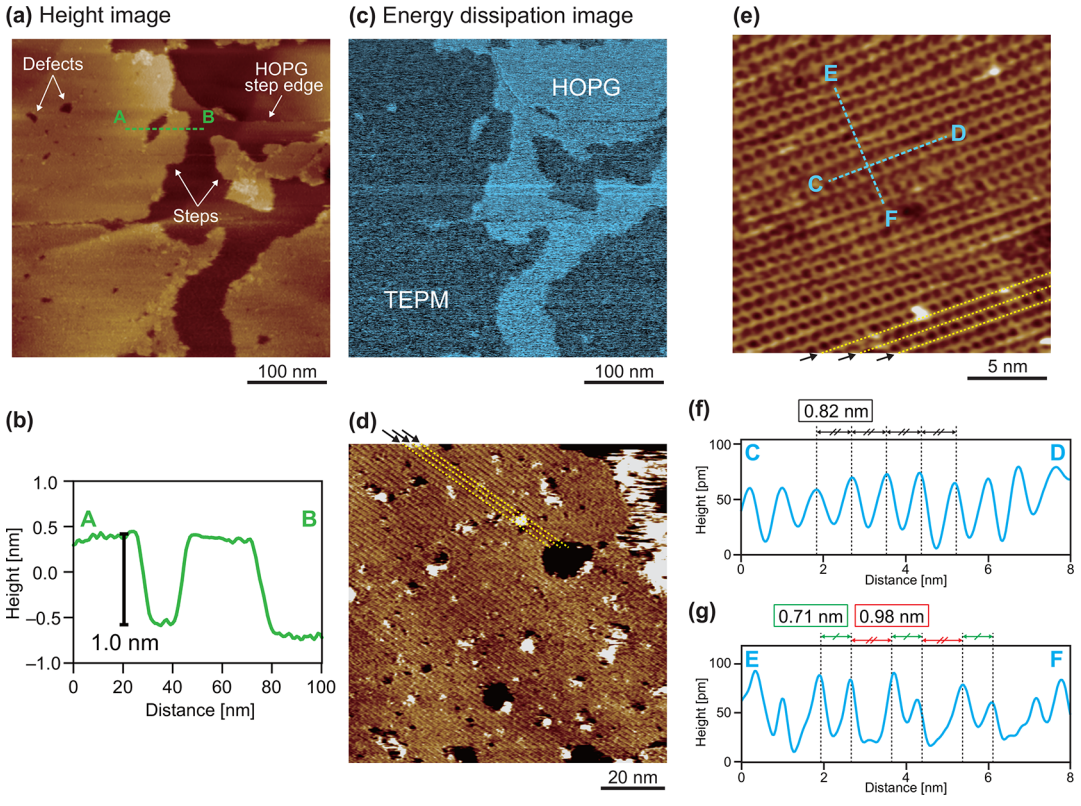

Figure 2. FM-AFM imaging of the TEPM molecules on the HOPG surface in water. (a) Height image. (b) Height profile obtained along line AB in (a), suggesting a step height of approximately 1 nm. (c) Energy dissipation image. (d) Molecular-scale FM-AFM image taken in an area of the TEPM monolayer. Dashed arrows indicate the molecular-scale striped contrasts. (e) High-resolution FM-AFM image of the TEPM monolayer. Molecular-scale striped contrasts similar to that observed in (d) appeared as indicated by the dashed arrows. (f, g) Height profiles obtained along line CD (f) and line EF (g) in (e).

https://dx.doi.org/10.1021/acs.jpcc.9b11246
J. Phys. Chem. C 2020, 124, 7760−7767

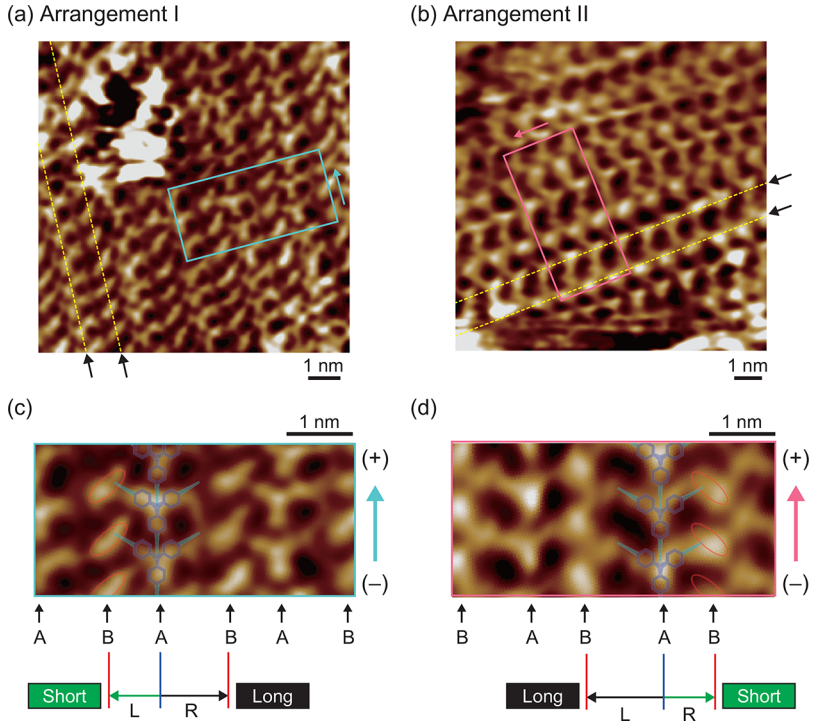

Figure 3. FM-AFM images of the TEPM monolayers with two different molecular arrangements. (a) and (b) show the FM-AFM images of arrangements I and II, respectively. (c) and (d) were cut out from the boxed areas indicated in (a) and (b), respectively. Molecular rows with two types of characteristic contrast were observed in both arrangements. Molecular rows with the three-point star (TPS)-like contrasts are defined to be in row A, whereas the others are defined as row B. In addition, the direction of row A is defined such that the TPS-like contrasts are aligned with vertically arranged Y letters.

μL) was immediately added to the rotating HOPG substrate. After drying for 30 s under rotation, the rotation was stopped, and the surface of the HOPG substrate was covered with ultrapure water (90 μL) to avoid contamination from the air. The substrate was then rinsed three times with ultrapure water (90 μL).

FM-AFM Measurements in Liquid. A laboratory-built AFM equipped with an ultralow noise deflection sensor[18,21] and a commercially available AFM controller (ARC 2, Oxford Instruments) were used for FM-AFM imaging. A Nanonis OC4.5 instrument (SPECS GmbH) was used as a frequency shift detector and an excitation controller of the cantilever vibration. The tip side of a PPP-NCHAuD cantilever (nominal spring constant = 42 N/m, Nanoworld AG) was coated with Si (30 nm) using a magnetron sputter coater (QT150, Quorum Technologies) prior to the AFM experiments.[22] The cantilever was oscillated at the near-resonance frequency using a photothermal excitation method.[21] All FM-AFM measurements were performed in ultrapure water at 25 °C.

DFT Calculations. To assess the stabilities of different adsorption configurations of a TEPM molecule on the HOPG surface, first-principles DFT calculations were performed using the Vienna ab initio simulation package (VASP), version 5.3.5.[23,24] All DFT calculations employed the projector augmented wave (PAW) method[25] with a cutoff energy of 450 eV and a generalized gradient approximation (GGA). In addition, to account for the dispersion correction in long-range interactions between TEPM and the HOPG surface, the optB88-vdW exchange-correlation functional (an optimized Becke88 functional integrated with a nonlocal vdW-DF correlation) developed by Klimeš et al. was used[26−30] after benchmark calculations had been performed, as described in the Supporting Information (Table S1). HOPG was modeled by a three-layer periodic p(8 × 8) slab of a (0001) surface, which contains 384 carbon atoms in total. A vacuum thickness of 25 Å above the top layer was chosen so that the interactions between repeated slabs were small. The conjugate-gradient algorithm was used to relax the ions into positions at local-minimum geometries. To ensure efficient DFT calculations without compromising the accuracy,[31−33] the bottom HOPG layer was fixed at the configuration of the optimized bulk lattice, while the two topmost layers and the adsorbate (TEPM molecule) were allowed to move during geometry optimization.

RESULTS AND DISCUSSION

Formation of TEPM Monolayers via Spin Coating. A spin-coating method described in the Methods section was employed to form self-assembled monolayers of TEPM molecules on the HOPG surface. Figure 2 shows the obtained FM-AFM images of the self-assembled monolayers prepared using a 0.6 mM solution of TEPM in chloroform. In the height image (Figure 2a), flat layered structures with clear steps and defects are observed. When TEPM molecules with a height of 1 nm form monolayers, the thickness of the layered structures should be approximately 1 nm. Indeed, the height profile along the AB line (Figure 2b) shows that the thickness was approximately 1 nm, as expected. In addition, Figure 2c shows the energy dissipation image obtained simultaneously with the FM-AFM height image. Clear contrasts of energy dissipations appeared between the lower and higher areas of the height image (Figure 2a), suggesting that the two areas consist of different chemical structures. Figure 2d shows an FM-AFM image obtained in the higher area. Surface structures

https://dx.doi.org/10.1021/acs.jpcc.9b11246
J. Phys. Chem. C 2020, 124, 7760−7767

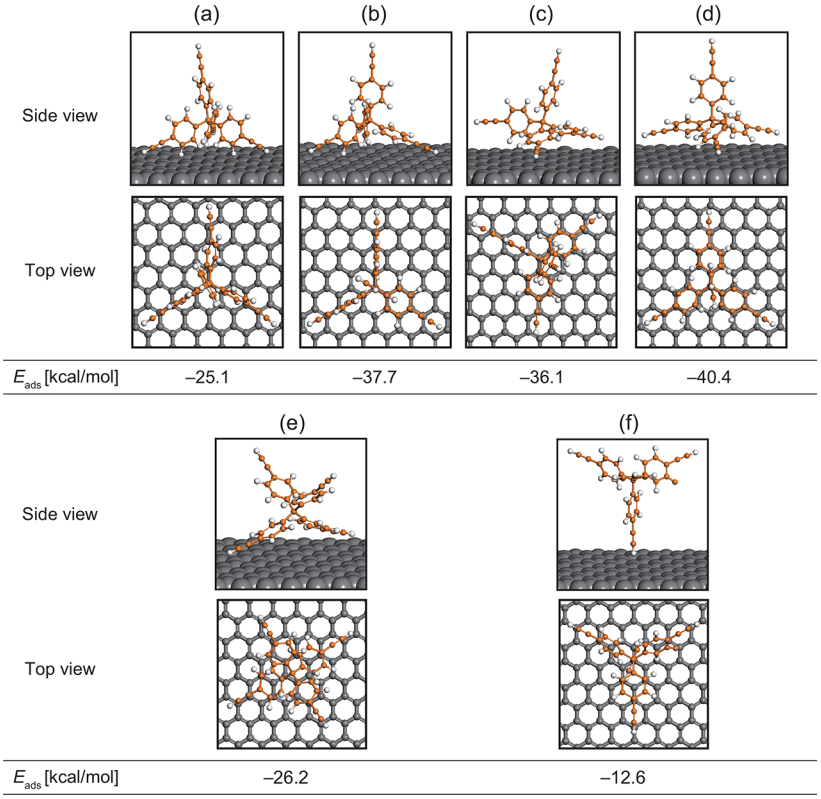

Figure 4. DFT calculation of the adsorption energy of a TEPM molecule on the HOPG surface.

with a striped pattern as indicated by the dashed lines with arrows in Figure 2d were visualized only in these higher areas. These results therefore suggest that the lower and higher areas correspond to the HOPG surface and the TEPM monolayers. We then examined how the concentration of the TEPM solution affects monolayer formation. When the TEPM concentration was increased beyond 1.0 mM, TEPM aggregates were observed (see the Supporting Information, Figure S1). As a result of the examination, the 0.6 mM TEPM concentration was found to be optimal for the highly reproducible formation of TEPM monolayers on HOPG. The existence of adsorbed TEPM molecules on HOPG surface was confirmed by attenuated total reflection Fourier transform infrared (ATR-IR) spectroscopy as shown in the Supporting Information (Figure S2). Figure 2e shows the high-resolution FM-AFM image obtained at the surface of the TEPM monolayer. In addition to the striped pattern that was also observed in Figure 2d, periodic structures appeared along the striped pattern in Figure 2e. Figure 2f,g shows the height profiles measured along lines CD and EF in Figure 2e. The average values and standard deviations (s.d.) of molecular spacings were determined by analyzing peak-to-peak distances in the height profiles. The height profile suggests that the spacing of periodic structures along the striped patterns (average value: 0.82 nm, s.d.: 0.05, n = 15) is somewhat smaller than the side length of the TEPM tetrahedral structure (*i.e.*, 1.3 nm, see Figure 1). This result suggests that the TEPM molecules formed linear molecular rows with highly packed structures. The height variations (less than 100 pm) were 1 order of magnitude smaller than the actual size of TEPM molecule as shown in Figure 2f,g. It is caused by a tip artifact due to the geometry of the tip apex. Since the macroscopic size of the tip apex is larger than the size of valleys between the highly packed TEPM molecules, the AFM tip cannot trace completely the bottom of the valleys. Thus, the molecules are visualized with small height variations than the actual surface variations. In contrast to the regular spacing in the CD direction, the height profile measured along the EF line reveals that there are two alternating spacings in the direction perpendicular to the linear rows [average value (short): 0.71 nm, s.d.: 0.05 nm, and n = 15 and average value (long): 0.98 nm, s.d.: 0.08 nm, and n = 15]. The spacings agreed well with the multiples of an HOPG lattice unit cell **b** (*i.e.*, 3**b** = 0.738 nm and 4**b** = 0.984 nm) as shown in Figure 2g. However, the experimentally determined values include errors due to thermal drift and scanner hysteresis. Thus, an assignment of molecular arrangements based on the experimental values should be carefully discussed. Models of molecular arrangements expected from the FM-AFM images will be shown and discussed later.

Subnanometer-Scale Structures in the FM-AFM Images. To better understand the arrangements and orientations of the TEPM molecules in the monolayers, we analyzed the subnanometer-scale structures visualized in the FM-AFM images (Figure 3). At the subnanometer resolution, not only were periodic structures attributed to the arrangements of TEPM molecules visualized, but characteristic intramolecular structures were also found. The same subnanometer-scale structures with periodicity were observed only in the directions indicated by the dashed lines in Figure 3a,b. These results suggest that the stripe pattern observed in Figure 2d,e originates from the parallel-oriented linear rows. Figure 3c,d shows cut-out images of the boxed areas indicated in Figure 3a,b, respectively. The cut-out FM-AFM images revealed that the intervals between molecular rows are not uniform. The molecular rows labeled row A show that clear

https://dx.doi.org/10.1021/acs.jpcc.9b11246
J. Phys. Chem. C 2020, 124, 7760−7767

three-point star (TPS) contrasts appear in every other row in the same orientation in both FM-AFM images. We therefore defined the plus and minus directions by likening the sequence of the TEPM molecule in a row to a series of "Y" alphabet letters and defining the upper side of Y as plus. Thus, double terminations of TPS-like contrasts indicate the upper (+) side. In contrast, the molecular rows of type B show tilted elliptic structures, suggesting that the TEPM rows form parallel arranged structures in an A-B-A repeating pattern. These rows of A and B types can be observed in Figure 3a,b. However, from the fact that the shorter and longer spacings appear in opposite ways in these figures, the two monolayers in Figure 3a,b should have different molecular arrangements, namely, arrangements I and II, respectively, as will be discussed in more detail later.

Orientation of TEPM Molecules and Determination of the Adsorption Energy by DFT Calculations. Due to its nonpolarity, TEPM should be oriented in such a manner that van der Waals interactions with the HOPG surface are maximized. Thus, the TEPM molecules are expected to exhibit orientations in which the three ethynylphenyl groups point toward the surface plane of HOPG. Indeed, as Figure 4 shows, models a−d in which three ethynylphenyl groups point toward the surface of HOPG are calculated as stable. In contrast, when a smaller number of ethynylphenyl groups [two in model e and one in model f] interact with the HOPG surface, the adsorption strengths are weaker with a loss of the interaction of one ethynylphenyl group with the surface depriving the system of adsorpton energy by approximately 10 kcal/mol. These DFT results suggest that three of the ethynylphenyl groups act as a tripod to interact with the HOPG surface.

A previous study reported that two stable configurations exist when two benzene molecules form a dimer, *i.e.*, the perpendicular and parallel configurations.[34] The interaction between a phenyl group of a TEPM molecule and a six-membered ring of HOPG may therefore have interaction patterns similar to those of the benzene dimer. To examine this prospect, we prepared the above-described four models (a−d) with different numbers of perpendicular and parallel interactions of the ethynylphenyl groups with the surface. In model a, all phenyl groups have perpendicular orientations, while in models b and c, the numbers of perpendicular phenyl groups are two and one, respectively, with the other phenyl groups having parallel orientations. In model d, all phenyl groups present a parallel orientation, although the planes of the phenyl groups are somewhat tilted in the form of a propeller to reduce steric hindrance. Of these four models, model d was calculated as the most stable. Although definite assignment of the molecular orientation is difficult because of the small energy differences of these models, our result seems to be reasonable because the symmetrical configuration of model d is consistent with the highly symmetrical TPS contrasts of row A observed in the FM-AFM images. It should be noted that the upward-pointing ethynylphenyl group has a relatively high flexibility compared with the three ethynylphenyl groups that interact directly with the HOPG surface, and thus the unbound ethynylphenyl group exhibits a small contribution to contrast formation in the subnanometer-resolution AFM images. As a result, the TEPM molecules give highly symmetrical TPS contrasts in row A arising from three equivalent phenyl groups over the surface. In contrast, the elliptic structures observed in row B (see Figure 3c,d) indicate that the TEPM molecules constituting row B have slightly tilted orientations.

Figure 5 shows a cut-out FM-AFM image at an area with the size of a single TEPM molecule (Figure 5a) in addition to the

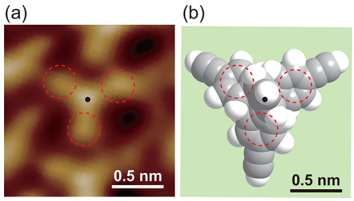

Figure 5. (a) Cut-out FM-AFM image and (b) space-filling model of a TEPM molecule with the same scale.

TEPM structure (Figure 5b) with the same scale where it is apparent that the characteristic TPS contrasts in the FM-AFM image agreed well with the structural features of TEPM molecules. Although the subnanometer-resolution imaging of organic molecules with a height of >1 nm is generally difficult even with STM, our results demonstrate that the FM-AFM technique is able to visualize intramolecular structures of small organic molecules, even those possessing large 3D structures.

Chiral Structures Based on Two Different Molecular Arrangements. To better characterize the two different molecular arrangements observed in the subnanometer-scale FM-AFM images (arrangements I and II in Figure 3a,b), we considered two models, as presented in Figure 6. The similarity between the projected TEPM structure and graphite allows us to superimpose the positions of the three six-membered rings of TEPM onto three six-membered rings of graphite, as illustrated in Figure 6a. The angles between molecular rows observed in the same FM-AFM image (see the Supporting Information, Figure S2) were 60°. These results indicate that the TEPM molecules are aligned by recognizing the surface structure of HOPG and achieving such superpositions in three different directions on the HOPG surface. However, since the lattice size of 2**a** (*i.e.*, 0.852 nm) and 3**b** (*i. e.*, 0.738 nm) is close to the experimentally determined value of the intermolecular distances (0.82 nm), there are two possibilities for the origin of the 0.82 nm spacing. The multiples of the single lattice unit, **a** and **b**, are shown in the Supporting Information (Table S2). Here, we consider two possibilities. If the spacing of 0.82 nm was to originate from the size of 3**b**, the error of the intermolecular distances in the direction of line CD in Figure 2e would be more than 10% as shown in the Supporting Information (Table. S3). In addition, the error in the direction of line EF (the direction perpendicular to line CD) would be more than 20%. These errors are too large even considering the influences of thermal drift and scanner hysteresis. In contrast, the errors become less than 4% if we assume that the spacing of 0.82 nm originates from the size of 2**a**. These considerations suggested that the lattice size of 2**a** is most likely the origin of the 0.82 nm spacing. Moreover, superimposing the positions of the three six-membered rings of TEPM onto three six-membered rings of graphite while considering the orientation of the TPS contrasts observed in the AFM images is possible only in the direction of **a**. Taken together, the TEPM molecules aligned along the direction of **a** with the spacing of 2**a**.

We subsequently focused on the intervals between rows A and B, which allowed us to find two different arrangements, namely, I and II. As shown in Figure 3c,d, both arrangements I and II exhibited parallel molecular rows that are arranged in an

https://dx.doi.org/10.1021/acs.jpcc.9b11246
J. Phys. Chem. C 2020, 124, 7760−7767

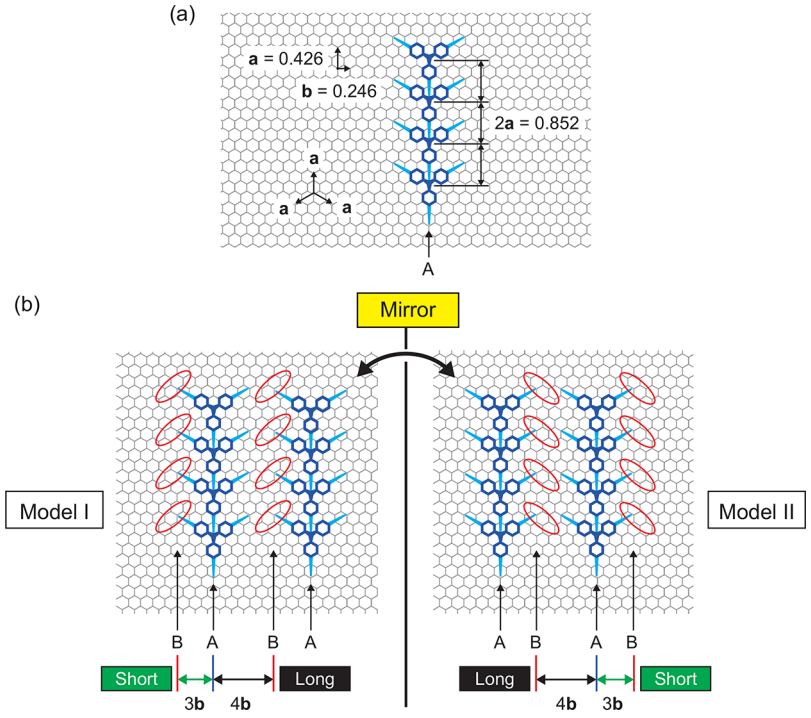

Figure 6. (a) Structure of row A assigned based on the subnanometer-resolution FM-AFM images. (b) Models I and II of the TEPM structures on the HOPG surface were constructed for arrangements I and II as shown in Figure 3.

A-B-A repeating manner. In both arrangements, the spacing between rows A and B is not uniform as short and long distances appear in alternating fashions. These results agreed with the two alternating spacings found in the perpendicular direction with respect to the striped pattern (Figure 2e,d). Closer inspection reveals that, in arrangement I (Figure 3a,c), in each of the B-A-B rows, the first B-A distance is shorter than the second A-B distance, whereas in arrangement II, the pattern was reversed. Based on the characteristic molecular-scale structures observed in the FM-AFM images, the expected arrangement models were constructed and labeled models I and II (Figure 6b), which correspond to arrangements I and II (Figures 3a,b). As such, the two alternating intervals between molecular rows are found to be 0.71 and 0.98 nm. These observed intervals agree well with three- and four-time distances of the repeating unit of the **b** direction, thereby suggesting that rows A and B are aligned with the distances of 3**b** and 4**b** (*i. e.*, 0.738 and 0.984 nm). Importantly, models I and II exhibit a mirror-image relationship between each other (Figure 6b). Our results therefore demonstrate that the 3D achiral TEPM molecules can form two types of chiral monolayers on the HOPG surface.

CONCLUSIONS

We herein reported our investigation into the molecular-scale arrangements of tetrakis(4-ethynylphenyl)methane (TEPM) molecules on a HOPG surface through FM-AFM experiments carried out in water. The subnanometer-resolution FM-AFM images revealed that the self-assembled monolayers of TEPM molecules could be classified into two types of chiral monolayers with a mutual mirror-image symmetry relationship in terms of molecular arrangements. In contrast to previously reported 2D organic molecules, the TEPM molecules exhibit 3D shapes. Furthermore, DFT calculations showed that, on the HOPG, three of the ethynylphenyl groups of a TEPM molecule act as a tripod upon adsorption, whereas the remaining ethynylphenyl group shows a vertical orientation. The ethynyl structure is a major cross-linkable group by well-established reactions such as the copper(I)-catalyzed alkyne-azide cycloaddition. Thus, molecular design based on the TEPM molecules may allow us to construct interfacial architectures extending toward the 3D interfacial space by introducing functional chemical structures to the vertically oriented ethynylphenyl groups. Of particular interest is the fact that TEPM monolayers of two different chiralities and with a mirror-image symmetry relationship are formed on the HOPG through the use of achiral TEPM molecules. Such 3D building blocks based on TEPM molecules should be useful in the design of interfacial architectures extending toward the 3D interfacial space.

ASSOCIATED CONTENT

Supporting Information

The Supporting Information is available free of charge at https://pubs.acs.org/doi/10.1021/acs.jpcc.9b11246.

FM-AFM images for optimization of the TEPM concentration (Figure S1), ATR-IR spectra (Figure S2) and orientations of the striped pattern in an FM-AFM image (Figure S3), benchmark DFT calculations (Table S1), the size of the HOPG lattice unit (Table S2), and errors in two possible assignment of molecular arrangements (Table S3) (PDF)

AUTHOR INFORMATION

Corresponding Author

Hitoshi Asakawa − *Nanomaterials Research Institute (NanoMaRi), Nano Life Science Institute (WPI-NanoLSI), and Division of Material Chemistry, Kanazawa University,*

https://dx.doi.org/10.1021/acs.jpcc.9b11246
J. Phys. Chem. C 2020, 124, 7760−7767

Kanazawa 920-1192, Japan; orcid.org/0000-0002-2320-2655; Email: hi_asa@staff.kanazawa-u.ac.jp

Authors

Sayaka Matsui − *Division of Material Chemistry, Kanazawa University, Kanazawa 920-1192, Japan*

Quang Thang Trinh − *Institute of Research and Development, Duy Tan University, Danang 550000, Vietnam;* orcid.org/0000-0002-3311-4691

Hajime Hirao − *Department of Chemistry, City University of Hong Kong, Kowloon, Hong Kong, China;* orcid.org/0000-0002-8239-3471

Yasuhide Inokuma − *Division of Applied Chemistry, Faculty of Engineering and Institute for Chemical Reaction Design and Discovery (WPI-ICReDD), Hokkaido University, Sapporo, Hokkaido 060-8628, Japan;* orcid.org/0000-0001-6558-3356

Tomoki Ogoshi − *Nano Life Science Institute (WPI-NanoLSI), Kanazawa University, Kanazawa 920-1192, Japan; Department of Synthetic Chemistry and Biological Chemistry, Graduate School of Engineering, Kyoto University, Kyoto 615-8510, Japan;* orcid.org/0000-0002-4464-0347

Saki Tanaka − *Division of Material Chemistry, Kanazawa University, Kanazawa 920-1192, Japan*

Kayo Komatsu − *Division of Material Chemistry, Kanazawa University, Kanazawa 920-1192, Japan*

Akio Ohta − *Division of Material Chemistry, Kanazawa University, Kanazawa 920-1192, Japan*

Tsuyoshi Asakawa − *Division of Material Chemistry, Kanazawa University, Kanazawa 920-1192, Japan*

Takeshi Fukuma − *Nano Life Science Institute (WPI-NanoLSI), Kanazawa University, Kanazawa 920-1192, Japan;* orcid.org/0000-0001-8971-6002

Complete contact information is available at: https://pubs.acs.org/10.1021/acs.jpcc.9b11246

Notes

The authors declare no competing financial interest.

■ ACKNOWLEDGMENTS

We acknowledge financial support from JST PRESTO, Japan (grant nos. JPMJPR1411 to H.A., JPMJPR141B to H.H., JPMJPR1311 to Y.I., and JPMJPR1313 to T.O.). This work was partially supported by JSPS KAKENHI (grant nos. JP17K17760 and JP17KK0112 to H.A.). H.A. and T.O. also acknowledge support by JST CREST (grant no. JPMJCR18R3). H.A, Y.I., and T.O acknowledge support by World Premier International Research Center Initiative (WPI), MEXT, Japan. H.H. also acknowledges support from the City University of Hong Kong (grant no. 9610369).

■ REFERENCES

(1) Stepanow, S.; Lingenfelder, M.; Dmitriev, A.; Spillmann, H.; Delvigne, E.; Lin, N.; Deng, X.; Cai, C.; Barth, J. V.; Kern, K. Steering Molecular Organization and HostGuest Interactions Using Two-Dimensional Nanoporous Coordination Systems. *Nat. Mater.* **2004**, *3*, 229−233.

(2) Blunt, M. O.; Russell, J. C.; del Carmen Gimenez-Lopez, M.; Taleb, N.; Lin, X.; Schröder, M.; Champness, N. R.; Beton, P. H. Guest-Induced Growth of a Surface-Based Supramolecular Bilayer. *Nat. Chem.* **2011**, *3*, 74−78.

(3) Gong, J.-R.; Wan, L.-J. Two-Dimensional Assemblies of Banana-Shaped Liquid Crystal Molecules on HOPG Surface. *J. Phys. Chem. B* **2005**, *109*, 18733−18740.

(4) Otsuki, J.; Shimizu, S.; Fumino, M. Self-Assembled Two-Dimensional Ordered Arrays of Tripod-Type Molecules on Graphite. *Langmuir* **2006**, *22*, 6056−6059.

(5) Lee, D.-W.; Kim, T.; Lee, M. An Amphiphilic Pyrene Sheet for Selective Functionalization of Graphene. *Chem. Commun.* **2011**, *47*, 8259−8261.

(6) Mann, J. A.; Rodríguez-López, J.; Abruña, H. D.; Dichtel, W. R. Multivalent Binding Motifs for the Noncovalent Functionalization of Graphene. *J. Am. Chem. Soc.* **2011**, *133*, 17614−17617.

(7) Cai, L.; Wang, L.; Kang, S.; Geng, Y.; Deng, K.; Zheng, Q.; Zeng, Q. Supramolecular Self-Assembly of Hexaphenylbenzene Derivatives with Different Symmetry and Number of Carboxylic Acid at Liquid/Solid Interfaces. *J. Phys. Chem. C* **2016**, *120*, 27259−27267.

(8) Fu, C.; Lin, H.-p.; Macleod, J. M.; Krayev, A.; Rosei, F.; Perepichka, D. F. Unravelling the Self-Assembly of Hydrogen Bonded NDI Semiconductors in 2D and 3D. *Chem. Mater.* **2016**, *28*, 951−961.

(9) Liu, X.-P.; Xue, L.-W.; Wei, Q.; Liang, M.; Deng, K.; Zhang, Z.-J.; Jiang, P. Seeing Modulability Self-assembled Monolayers of π-Conjugated Perylene Derivatives by Scanning Tunneling Microscopy. *J. Phys. Chem. C* **2016**, *120*, 18607−18615.

(10) Weigelt, S.; Busse, C.; Petersen, L.; Rauls, E.; Hammer, B.; Gothelf, K. V.; Besenbacher, F.; Linderoth, T. R. Chiral Switching by Spontaneous Conformational Change in Adsorbed Organic Molecules. *Nat. Mater.* **2006**, *5*, 112−117.

(11) Elemans, J. A. A. W.; De Cat, I.; Xu, H.; De Feyter, S. Two-Dimensional Chirality at LiquidSolid Interfaces. *Chem. Soc. Rev.* **2009**, *38*, 722−736.

(12) Raval, R. Chiral Expression from Molecular Assemblies at Metal Surfaces: Insights from Surface Science Techniques. *Chem. Soc. Rev.* **2009**, *38*, 707−721.

(13) Chen, T.; Yang, W.-H.; Wang, D.; Wan, L.-J. Globally Homochiral Assembly of TwoDimensional Molecular Networks Triggered by Co-Absorbers. *Nat. Commun.* **2013**, *4*, 1389.

(14) Cao, H.; Tahara, K.; Itano, S.; Tobe, Y.; De Feyter, S. Odd-Even Effects in Chiral Phase Transition at the Liquid/Solid Interface. *J. Phys. Chem. C* **2017**, *121*, 10430−10438.

(15) Destoop, I.; Minoia, A.; Ivasenko, O.; Noguchi, A.; Tahara, K.; Tobe, Y.; Lazzaroni, R.; De Feyter, S. Transfer of Chiral Information from a Chiral Solvent to a Two-Dimensional Network. *Faraday Discuss.* **2017**, *204*, 215−231.

(16) Zaera, F. Chirality in Adsorption on Solid Surfaces. *Chem. Soc. Rev.* **2017**, *46*, 7374−7398.

(17) Huan, J.; Zhang, X.; Zeng, Q. Two-Dimensional Supramolecular Crystal Engineering: Chirality Manipulation. *Phys. Chem. Chem. Phys.* **2019**, *21*, 11537−11553.

(18) Fukuma, T.; Kobayashi, K.; Matsushige, K.; Yamada, H. True Atomic Resolution in Liquid by Frequency-Modulation Atomic Force Microscopy. *Appl. Phys. Lett.* **2005**, *87*, No. 034101.

(19) Asakawa, H.; Ikegami, K.; Setou, M.; Watanabe, N.; Tsukada, M.; Fukuma, T. Submolecular-Scale Imaging of α-Helices and C-Terminal Domains of Tubulins by Frequency Modulation Atomic Force Microscopy in Liquid. *Biophys. J.* **2011**, *101*, 1270−1276.

(20) Ido, S.; Kimura, K.; Oyabu, N.; Kobayashi, K.; Tsukada, M.; Matsushige, K.; Yamada, H. Beyond the Helix Pitch: Direct Visualization of Native DNA in Aqueous Solution. *ACS Nano* **2013**, *7*, 1817−1822.

(21) Fukuma, T. Wideband Low-Noise Optical Beam Deflection Sensor with Photothermal Excitation for Liquid-Environment Atomic Force Microscopy. *Rev. Sci. Instrum.* **2009**, *80*, No. 023707.

(22) Akrami, S. M. R.; Nakayachi, H.; Watanabe-Nakayama, T.; Asakawa, H.; Fukuma, T. Significant Improvements in Stability and Reproducibility of Atomic-Scale Atomic Force Microscopy in Liquid. *Nanotechnology* **2014**, *25*, 455701.

(23) Kresse, G.; Furthmüller, J. Efficiency of Ab-Initio Total Energy Calculations for Metals and Semiconductors Using a Plane-Wave Basis Set. *Comput. Mater. Sci.* **1996**, *6*, 15−50.

(24) Kresse, G.; Hafner, J. Ab initiomolecular dynamics for liquid metals. *Phys. Rev. B* **1993**, *47*, 558−561.

(25) Blöchl, P. E. Projector Augmented-Wave Method. *Phys. Rev. B* **1994**, *50*, 17953−17979.
(26) Trinh, Q. T.; Nguyen, A. V.; Huynh, D. C.; Pham, T. H.; Mushrif, S. H. Mechanistic Insights into the Catalytic Elimination of Tar and the Promotional Effect of Boron on It: First-Principles Study Using Toluene As a Model Compound. *Catal. Sci. Technol.* **2016**, *6*, 5871−5883.
(27) Klimeš, J.; Bowler, D. R.; Michaelides, A. Chemical Accuracy for the Van der Waals Density Functional. *J. Phys.: Condens. Matter* **2010**, *22*, No. 022201.
(28) Klimeš, J.; Bowler, D. R.; Michaelides, A. Van der Waals Density Functionals Applied to Solids. *Phys. Rev. B* **2011**, *83*, 195131.
(29) Mohan, O.; Trinh, Q. T.; Banerjee, A.; Mushrif, S. H. Predicting CO_2 adsorption and reactivity on transition metal surfaces using popular density functional theory methods. *Mol. Simul.* **2019**, *45*, 1163−1172.
(30) Sarkar, C.; Pendem, S.; Shrotri, A.; Dao, D. Q.; Pham Thi Mai, P.; Nguyen Ngoc, T.; Chandaka, D. R.; Rao, T. V.; Trinh, Q. T.; Sherburne, M. P.; et al. Interface Engineering of Graphene-Supported Cu Nanoparticles Encapsulated by Mesoporous Silica for Size-Dependent Catalytic Oxidative Coupling of Aromatic Amines. *ACS Appl. Mater. Interfaces* **2019**, *11*, 11722−11735.
(31) Trinh, Q. T.; Chethana, B. K.; Mushrif, S. H. Adsorption and Reactivity of Cellulosic Aldoses on Transition Metals. *J. Phys. Chem. C* **2015**, *119*, 17137−17145.
(32) Trinh, Q. T.; Banerjee, A.; Yang, Y.; Mushrif, S. H. Sub-Surface Boron-Doped Copper for Methane Activation and Coupling: First-Principles Investigation of the Structure, Activity, and Selectivity of the Catalyst. *J. Phys. Chem. C* **2017**, *121*, 1099−1112.
(33) Nandula, A.; Trinh, Q. T.; Saeys, M.; Alexandrova, A. N. Origin of Extraordinary Stability of Square-Planar Carbon Atoms in Surface Carbides of Cobalt and Nickel. *Angew. Chem., Int. Ed.* **2015**, *54*, 5312−5316.
(34) Tsuzuki, S.; Honda, K.; Uchimaru, T.; Mikami, M.; Tanabe, K. Origin of Attraction and Directionality of the π/π Interaction: Model Chemistry Calculations of Benzene Dimer Interaction. *J. Am. Chem. Soc.* **2002**, *124*, 104−112.

https://dx.doi.org/10.1021/acs.jpcc.9b11246
J. Phys. Chem. C 2020, 124, 7760−7767